# Soils in Karst Sinkholes Record the Holocene History of Local Forest Fires at the North of European Russia

**Nikita Mergelov [1],\*, Dmitry Petrov [1], Elya Zazovskaya [1], Andrey Dolgikh [1] ,
Alexandra Golyeva [1], Vladimir Matskovsky [1], Renat Bichurin [1], Sofia Turchinskaya [1],
Vladimir Belyaev [1,2] and Sergey Goryachkin [1]**

[1] Institute of Geography, Russian Academy of Sciences, 119017 Moscow, Russia; pd437807@mail.ru (D.P.);
    zazovskaya@igras.ru (E.Z.); dolgikh@igras.ru (A.D.); golyeva@igras.ru (A.G.); matskovsky@igras.ru (V.M.);
    terpomo@bk.ru (R.B.); turchinskaya@igras.ru (S.T.); vladimir.r.belyaev@gmail.com (V.B.);
    goryachkin@igras.ru (S.G.)
[2] Faculty of Geography, Lomonosov Moscow State University, 119991 Moscow, Russia
\*   Correspondence: mergelov@igras.ru

check for updates

**Abstract:** Despite the abundance of charcoal material entrapped in soils, they remain relatively less studied pyrogenic archives in comparison to the sedimentary paleofire records (e.g., lacustrine and peat deposits), and that is especially the case in most of Russia's territory. We report here on the deep soil archives of the Holocene forest fires from the Pinega District of the Arkhangelsk region (64.747° N, 43.387° E). Series of buried soil profiles separated by charcoal layers and clusters were revealed in specific geomorphological traps represented by the active and paleokarst subsidence sinkholes on sulfate rocks overlaid by glacial and fluvial deposits. We combine the study of soil morphology and stratigraphy with a set of radiocarbon data on charcoal and soil organic matter, as well as the anthracomass analysis, to extract a set of paleoenvironmental data. A total of 45 radiocarbon dates were obtained for the macrocharcoal material and the soil organic matter. The maximum temporal "depth" of archives estimated from the radiocarbon dating of macrocharcoal reached 10,260 ± 35 cal yr BP. Soil formation with Podzols established at the inter-pyrogenic stages repeatedly reproduced within the period of ten thousand years, while the dominant tree species was *Pinus* sp. According to the macrocharcoal data, the intervals between fires have shortened in the last thousand years. Dendrochronological estimates suggest the occurrence of fires in almost every decade of the 20th and early 21st centuries. This is the first study of the millennia-scale soil record of forest fires in this particular region of Russia.

**Keywords:** paleofires; $^{14}$C AMS; soil archive; pyrogenic carbon; dendrochronological reconstruction

## 1. Introduction

Charcoal particles are ubiquitous in soils, and their analysis is a widely applied tool in paleoenvironmental studies including dynamics of forest ecosystems in the past [1–13]. Pyrogenic carbon (PyC) constitutes a significant portion of soil organic carbon, and in some soils its share exceeds 30% [14,15]. Charcoal material largely contributes to soil PyC [16] and is archived through burial mainly due to the post-pyrogenic erosion/deposition cycles [17,18], bioturbations by soil fauna and tree uprooting, cryoturbations (e.g., frost action and solifluction), and turbations with various anthropogenic origins [3,6,13]. While the microscopic charcoal is transported over longer distances and accumulates in lake sediments and peatlands providing the regional and local fire background level [19–23], most of the macroscopic charcoal particles are archived in situ [24] or at distances of less than 50 m from the initial burn [25]. Regular meso- and microtopography patterns raise the probability

that most of the macrocharcoal material will be trapped locally. Ohlson and Tryterud [24] found that charcoal particles of >0.5 mm in forest soils provide a reliable evidence for local pyrogenic events, and their occurrence helps to discriminate between fire-prone and fire-free areas with high spatial resolution. Macroscopic charcoal data could offer an estimate of the minimum number of past fire events in a given stand when the number of sampling soil pits is sufficient. However, the reliability of such estimate rises when the macrocharcoal data are compared with the ex situ evidence from microcharcoal accumulations in sediments [6] and controlled by dendrochronological datasets [23].

Wood charcoal is an appropriate material for radiocarbon dating because of its resistance to decay, large proportion of chemically inert carbon, and robust separation from other soil material [3]. However, charcoal taphonomy usually exhibits complex patterns in soils, and accurate estimates of time-since-fire intervals are not always possible [2]. Charcoal originates from various parts of the trees, like trunks, branches, and roots, and when produced from the older wood (more than 200 years old) could cause a significant "inbuilt age" effect on the accuracy of time-since-fire estimates [2].

The fire history research based on sediment/soil charcoal data has advanced rapidly [26,27], with an extensive dataset already available through the Global Charcoal Database (www.paleofire.org). It aggregates information on paleofires for the last 22 thousand years and clearly indicates the gaps in data for Russia, with only a few sampling locations present. The number of paleofire studies conducted on Russian territory has recently began to rise, e.g., in Meshchera Lowlands (Ryazan Region) [12,22,28], Kaluga Region [29], Komi Republic [21], Karelia [23], and on the western Siberian plain (Tomsk region) [30], with only a few studies specifically focused on soil charcoal records e.g., [13]. Although the soil charcoal archives are studied to a lesser extent than lake and peat deposits, they could aid our understanding of paleofire dynamics, rates of soil formation, and development of forest ecosystems at the inter-pyrogenic stages.

The charcoal-rich archives of forest paleofires are more readily formed in the meso- and microtopography depressions, that often demonstrate buried soil profiles associated with the repeated post-fire episodes of erosion and deposition. In this sense, it is the karst landscape that could offer a unique regular network of pedosedimentary sequences, which reveal phases of soil formation, e.g., [31,32], with a high spatial resolution. The grid of closed geomorphological traps granted by a karst landscape can capture the bulk of the macrocharcoal material produced locally and offer a record of spatially close pyrogenic and depositional events. We selected the fields of closed subsidence sinkholes in a karst landscape of the Pinega district, in the Arkhangelsk region (north of European Russia), to test this hypothesis.

The objective of this study is to evaluate the series of buried soils in karst sinkholes of various sizes and shapes as in situ archives of the forest paleofires and to test their capacity to reconstruct the long-term history of local fires. We hypothesize that deep soil archives were formed throughout the Holocene by the post-fire erosion-deposition processes complemented by the regular uprooting events due to windthrows and tree falls.

For the study region, the forest fire history has been previously reconstructed only for the last 200 years from the archive maps and Landsat imagery of the Pinega State Nature Reserve [33], which is adjacent to the key sites reported here, and the corresponding references. As far as we know, there are no studies of the deep soil archives in the region as potential sources of the long-term paleofire indicators. Here we combine the soil morphology study, anthracomass estimates, and chemical analyses with the $^{14}$C dating of macrocharcoal to start filling this gap and to get the first approximation of paleofire occurrence from the soil archives in the karst landscape of the Pinega district, in the Arkhangelsk region.

## 2. Materials and Methods

### 2.1. Study Area

The study area is within the northern part of the boreal forest zone, and the sampling sites are located on the right bank of the Pinega River, in the Upper-Kuloy Plain, Archangelsk Region, Russia.

This territory lies 5 km to the north of the Pinega settlement, belongs to the Pinega Forestry, and is adjacent to the Pinega State Nature Reserve (Figure 1).
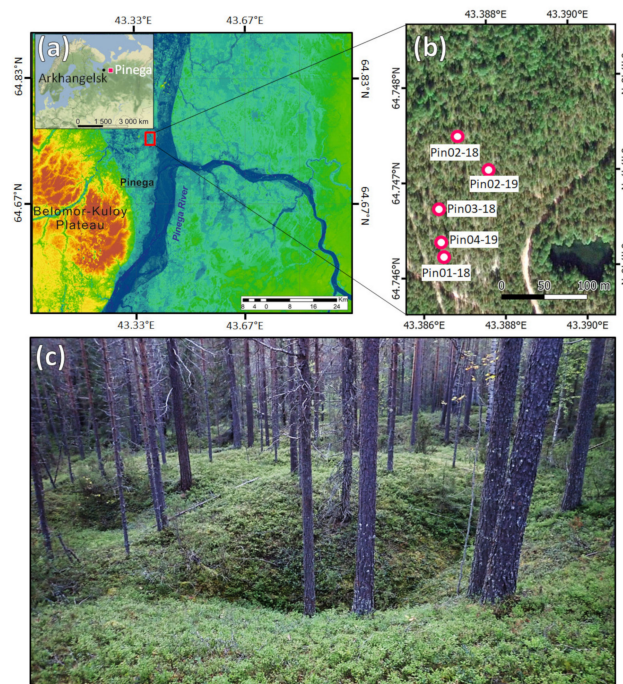


**Figure 1.** Study area (**a**) in the Pinega District, Arkhangelsk Region, Russia, N64.747°, E43.387°; (**b**) location of soil pits; (**c**) regular matrix of closed subsidence sinkholes in the karst landscape with *Pinus sylvestris* forest.

According to the local meteorological station, the climate is characterized by long and cold winters, relatively short and moderately warm and cloudy summers, and rather long springs and autumns with frequent temperature fluctuations. The mean annual air temperature is −0.2 °C, the air temperature in January is averaged at −13.9 °C and in July at +15.0 °C. The mean annual precipitation reaches 650 mm (55% occur during the warm season). The snow cover varies from 44 to 61 cm and the soil freezing depth is 75 cm. Meteorological observations in 1976–2000 revealed an increasing trend in the mean air temperatures and precipitation during the warm season [34].

The Pinega district combines the features of glaciated landscapes typical of the European North of Russia and unique, strongly karstified terrains formed on the hard gypsum bedrock, highly subjective to weathering [34]. This results in a dissected topography and a complicated structure of parent materials and soils. The karst formation began in the Mesozoic [35]. Continental glaciations in the Middle and Late Pleistocene dramatically affected karst landforms, which were covered by glacial deposits [35]. The last glacial maximum occurred in 18–16 ka BP, and the territory likely became ice-free in 13.7 ka BP [36]. In the Holocene, when the region did not experience glaciations, the conditions were in general favorable for karst processes that exhibited considerable fluctuations in their rates. The study sites are located in the area of covered karst, where the sulfate bedrock is overlaid by the glacial and fluvial deposits (mainly sands and sandy loams) with a thickness of up to 5 m, and gypsum outcrops occur only fragmentarily. The landforms with the subsidence sinkholes are well drained, since the surface runoff is partially converted into a subsurface one through active sinkhole channels. The sinkholes' spatial density varies between 400 and 1000 forms per km$^2$. Karstified territories are also affected by a set of contemporary karst and karst-related processes, such as denudation/accumulation, active linear and surface erosion, landslide and slope processes [34].

During the Holocene, the territory experienced the same climatic fluctuations as the whole forest zone of the European Russia [37,38].

The contemporary vegetation cover at the study sites located on the fields of the subsidence sinkholes is mainly represented by *Pinus sylvestris* with admixture of *Picea obovata*, *Vaccinium myrtillus*, *Vaccinium vitis-idaea*, *Pleurozium schreberi*, *Hylocomium splendens*, *Dicranum polysetum*, and spots of *Cladonia alpestris* in the ground cover. At the adjacent Pinega State Nature Reserve, the contemporary pine forests are also mainly confined to the karst landforms, although they were much more widespread in the past [39].

Both natural and human-induced forest fires occur in the region. Pinega is one of the earliest settlements in the Russian north, and anthropogenic influence has become noticeable here since the middle of the 12th century [40]. The previous population of Finnish tribes contrary to the Fennoscandia [41] was very scarce, their economy was based on hunting, fishing, and gathering without any agriculture [42,43] and was thus not likely to noticeably affect the forest fires. Until the end of 19th century, human activities were mostly based on haying, hunting, and fishing; no timber was harvested until the 1920s. Since 1960s, the areas of harvesting became widespread, but the natural processes of reforestation lessened the proportion of cleared territory [34]. At the same time, lightning-ignited forest fires are common in the region [33,44].

## 2.2. Soil Sampling

The samples were collected in the pine forest (*Pinus sylvestris*) with a regular network of cone-shaped sinkholes (Ø 10–25 m) of various subsidence levels, ranging from 0.5 to 5 m downward from the day surface of elevations in-between. We established soil pits in the three sinkholes of various subsidence levels and sizes:

(1)  in sinkhole Pin01–18 (N64.74635°, E43.38613°) with a flattened surface, peripheral slopes <10°, day surface Δ = 1 m, Ø 15 m, profile depth of 250 cm;

(2)  in sinkhole Pin02-18 (N64.74747°, E43.38674°) with steep peripheral slopes of 20–35°, day surface Δ = 5 m, Ø 25 m, profile depth of 120 cm;

(3)  in sinkhole Pin03-18 (N64.74696°, E43.38632°) with flattened surface, peripheral slopes <5°, day surface Δ = 0.5 m, Ø 10 m, profile depth of 140 cm.

The soil pits were also excavated on the residual surfaces between sinkholes:

(1)  Pin02-19 (N64.74739°, E43.38774°) with macroscopic charcoal buried due to the uprooting;

(2)  Pin04-19 (N64.74635°, E43.38613°) with no macroscopic signs of charcoal in the soil profile.

We hypothesized that the pyrogenic soil archives at the center, periphery, and high flat sides of the sinkholes are complementary to each other and sampled both the soils and charcoal-rich layers/clusters on these topography elements. The samples were collected along the entire soil profile in all horizons that were distinguished in the field upon their macromorphology.

Sulfate rocks always remained deeper than the maximum depth of soil pit excavated (250 cm), and the parent rock for soil formation was represented by the layers of fluvial and glacial sediments with no visible pedogenic features and no macroscopic accumulations of charcoal material.

## 2.3. Dendrochronological Reconstruction

The Scots pine trees (*Pinus sylvestris* L.) were examined around the soil pits within a radius of ~100 m. Samples were collected from 74 trees, when the visible fire scars or bumps on the bark that could serve as an indicator of a healed scar had been found. Both the core samples and partial cross-sections were taken by a chainsaw. The partial cross-sections were extracted by making two vertical cuts in the middle of the scar and at a ~10 cm distance from it, and two horizontal cuts at a distance of 3–5 cm. The cores were taken by an increment borer (core Ø 4.3 mm) in the center of the scar, and also on the right and left sides. We also sampled control cores that did not pass through the scar, and a core that included the control radius. We took GPS coordinates and photographs

of the trees and documented the height and orientation of the scars. We packed the cores in the special individual containers and marked them. In the laboratory, we fixed the cores onto wooden holders with PVA. After the glue had dried, we sanded the cores with sandpaper of steadily decreasing roughness to increase the contrast of the annual rings. We marked every 10th, 50th and 100th ring of the cores under a binocular [45] and scanned them on an Epson Perfection 10,000XL professional scanner with a resolution of 2800 dpi. The obtained images were processed in the Cybis CooRecorder software, and the width of the growth rings was measured with 0.01 mm accuracy. We cross-dated the obtained series of ring width measurements, first for different measurements of one tree, and then for different trees. We used visual cross-dating and descriptive statistics in the Cybis CDendro program. We checked the dates and quality of the measurements in the COFECHA program. All the tree-ring series were dated, i.e., a calendar year was assigned to each measured tree ring. A visual search for the fire scar damages was carried out. For each core, the date of the last annual ring before the damage was noted, and the date for the first ring after the scar was determined when possible.

*2.4. Charcoal and Soil Organic Matter Analyses*

The primarily methodological approach we employed was to evaluate all the macrocharcoal (>0.5 mm) that was sequestered in the soil and to use it as an in situ proxy of the local forest fires. 500–1100 cm$^3$ of soil samples taken from each unit of soil (pattern or horizon) were wet-sieved on a set of mesh sieves of 5 mm, 2 mm, 1 mm, and 0.5 mm to obtain estimates for the following anthracomass fractions: >5, 5–2, 2–1, 1–0.5 mm. The obtained samples were dried. When necessary, the charcoal fragments were additionally separated with soft tweezers from the bulk of the sieved sample under a Leica MZ6 binocular. The final fraction samples were weighed to calculate the charcoal concentration in mg of charcoal per kg of dry soil (= ppm), also known as specific anthracomass [1,5]. The taxonomic identification of charcoals was performed under reflected light with a Nikon Eclipse E200 microscope using Barefoot and Hankins [46], our charcoal reference collection, and a tree anatomy atlas [47]. The identification of small charcoal particles was conducted under a scanning electron microscope (JEOL JSM-6610LV, Institute of Geography RAS, Moscow, Russia) in a secondary electrons mode.

The content of total organic carbon (TOC), total nitrogen (TN), and carbon ($\delta^{13}$C) and nitrogen ($\delta^{15}$N) stable isotope ratio in charcoal (>5, 5–2, 2–1, 1–0.5 mm fractions) and soil samples (<2 mm) were determined using Vario ISOTOPE Cube CHNS-analyzer coupled for measurements of stable isotope ratios with Isoprime PrecisION IRMS (Elementar, Germany). For soil samples, inorganic C was removed with 1M HCl treatment and then rinsed in deionized water. Samples were dried with a Scientz-10N freeze dryer and crushed for homogenization in a Retsch Mixer Mill MM 400.

*2.5. Radiocarbon Analyses*

To avoid obtaining average dates from different fire events, discrete pieces of charcoal (>5 mm) were used for the radiocarbon dating. The extant morphology was important to date not mixed but individual particles. However, if charcoal was rare, we combined two or more proximal pieces. Charcoal was cleaned using acid-base-acid treatments. The graphitization and pressing of targets for $^{14}$C AMS were conducted in the Radiocarbon Laboratory of the Institute of Geography RAS (Moscow, Russia) with the automated graphitization system AGE 3 (Ionplus, Zurich, Switzerland). $^{14}$C AMS measurements were performed at the Center for Applied Isotope Studies of the University of Georgia (Athens, USA), using the CAIS 0.5MeV accelerator mass spectrometer. All dates were converted to calendar years before present (BP). The radiocarbon dates were calibrated in OxCal v.4.3.256 (https://c14.arch.ox.ac.uk/oxcal.html) [48], IntCal13 was used for the calibration curve [49], and the NH1 post-bomb calibration curve was used for modern radiocarbon [50]. A sum distribution resulting in a superposition of all the calibrated distributions was used as the common method for the aggregation of a large set of radiocarbon determinations.

The "inbuilt age" effect could be significant, and the actual age of a fire may not occur within the 2σ confidence interval of a calibrated $^{14}$C age of charcoal [2]. So, to reliably distinguish between

different fires, we also calculated the time distances between 2σ intervals (cal BP, 95.4% probability) for each ^{14}C determination in a row of consecutive pyrogenic events.

We also determined the radiocarbon age of TOC in soil samples (<2 mm, anthracomass removed) to compare with the radiocarbon age of charcoal in the same soil layers and to get a rough estimate of what the "inbuilt age" could be. Although, we are aware that there could be an opposite renovation effect on the radiocarbon age of soil TOC due to the migration of fresh organic matter into the soil.

## 3. Results

### 3.1. Morphology of Pyrogenic Soil Archive

The soil pyrogenic archives comprised series of Podzols and Arenosols [51] including those in burial state (Figure 2). Albic Podzol (Arenic) prevailed at the top of the soil sequences in the sinkhole traps. The buried soil material often contained individual buried profiles with the following horizon combination: AE(EA)-E-Bs(Bsh)-BC. Not every horizon from this sequence manifested in each buried profile, and often material of E and Bs horizons was mixed. During the field description, macrocharcoal particles demonstrated significantly higher abundances specifically in E horizons. Various signs of E, Bs and Bsh material in the form of discontinuous layers and clusters were also scattered through the bulk mineral mass that filled the sinkholes. Up to three charcoal layers were present in the litter horizons of the present-day surface. The central parts of sinkholes that are still draining the surface runoff contained the largest accumulations of buried charcoals in the form of bowls, wedges, and stripes (Figure 2a–e). The soils on residual surfaces between sinkholes (Figure 2f,g) contained only a few macrocharcoal assemblages, presumably due to the erosional processes that regularly removed charcoal. A substantial erosion impact was evident from the 2–3-fold difference in the total thickness of subsoil horizons at the high flats between sinkholes and at the central parts of sinkholes. The sequences of fluvial and glacial sediments started only from the depth of 55–95 cm at the high flats (Figure 2f,g), while in the sinkholes they were overlaid by a series of buried Podzols and Arenosols with a thickness of more than 200 cm. This indicates a long-term impact of denudation, along with the subsidence processes in this karst landscape, suggesting accumulation and denudation models of pedogenesis implemented at a very close distance.

### 3.2. Anthracomass

#### 3.2.1. Concentration

The soils in the central part of sinkholes are 10–13 times more enriched in anthracomass (17,400 ppm; Figure 3c,d) than the soils in the periphery of the sinkholes (max. 13,500 ppm; Figure 3a,b), located just 50 cm away from the center. On the meso- and microscale elevations in between sinkholes we observed a depletion in soil macrocharcoal (max. 2700 ppm): the concentration was 50–60 times lower than in soils of the central part of sinkholes, and five times lower than in soils in the periphery. A decline in the concentration of charcoal particles on elevations was rather gradual with depth, (Figure 3g) and no particles bigger than 1 mm were found at a depth of 45–50 cm. Some of the charcoal particles of a smaller fraction (<1 mm) still appeared in the parent rock sequences, suggesting vertical migration into fluvial and glacial sediments, which were formed prior to forest establishment and fire occurrence. However, the individual uprooting events could still enrich with charcoal the middle layers of soils on elevations (Figure 3h).
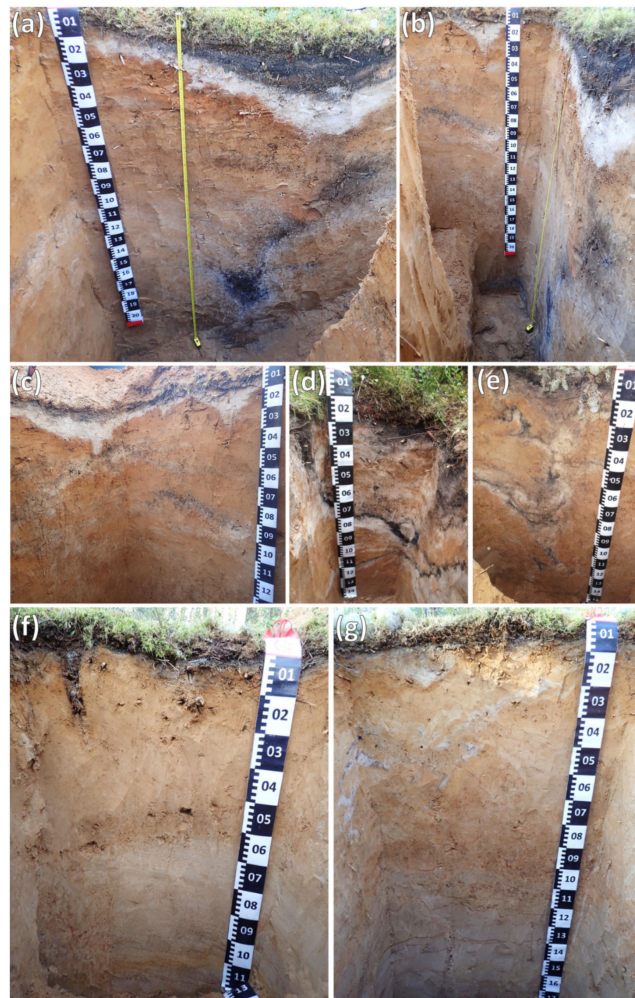
**Figure 2.** Pyrogenic archives in karst landscapes of the Pinega District (Arkhangelsk Region, Russia): (**a**) central part of large sinkhole Pin01-18, including charcoal clusters in the sinkhole channel zone; (**b,c**) periphery of sinkhole Pin01-18, with a lesser amount of buried charcoal; (**d**) central part of sinkhole Pin02-18; (**e**) central part of sinkhole Pin03-18, near the sinkhole channel zone; (**f**) Arenosol (Pin04-19) on residual surface between sinkholes with no signs of pedoturbations; (**g**) Podzol (Pin02-19) on residual surface between sinkholes with uprooting features and buried material from horizons E and Bs.

### 3.2.2. Botanical Identification

A total of 172 pieces of macrocharcoal were examined. Most of the macrocharcoal (86%) originated from the pine trees (*Pinus* sp.) (Table S1, Figure 4). Some charcoal pieces featured a characteristic luster that suggests a secondary combustion. The samples with signs of secondary combustion occurred more frequently in fractions with a smaller size (<2 mm). In a number of samples, the size of charcoal particles was very small and did not allow for an accurate identification of the species. Smaller samples were most often found in the deep horizons, starting from a depth of 200 cm from the modern-day surface. Overall, the taxonomic composition was poor. We did not identify fire-intolerant species, which usually dominate when the biomass burning is low. The samples were dominated by the fire-prone trees (*Pinus* sp.) normally more abundant during periods of higher fire activity with a share of fire-tolerant shrubs resistant to fires of moderate intensity, like *Juniperus* sp. Previously, Bobrovsky et al. [13] also documented the poor taxonomic composition of macrocharcoal in Podzols and Arenosols of the Meshchera Lowlands (Russia) with the dominance of *Pinus sylvestris*.
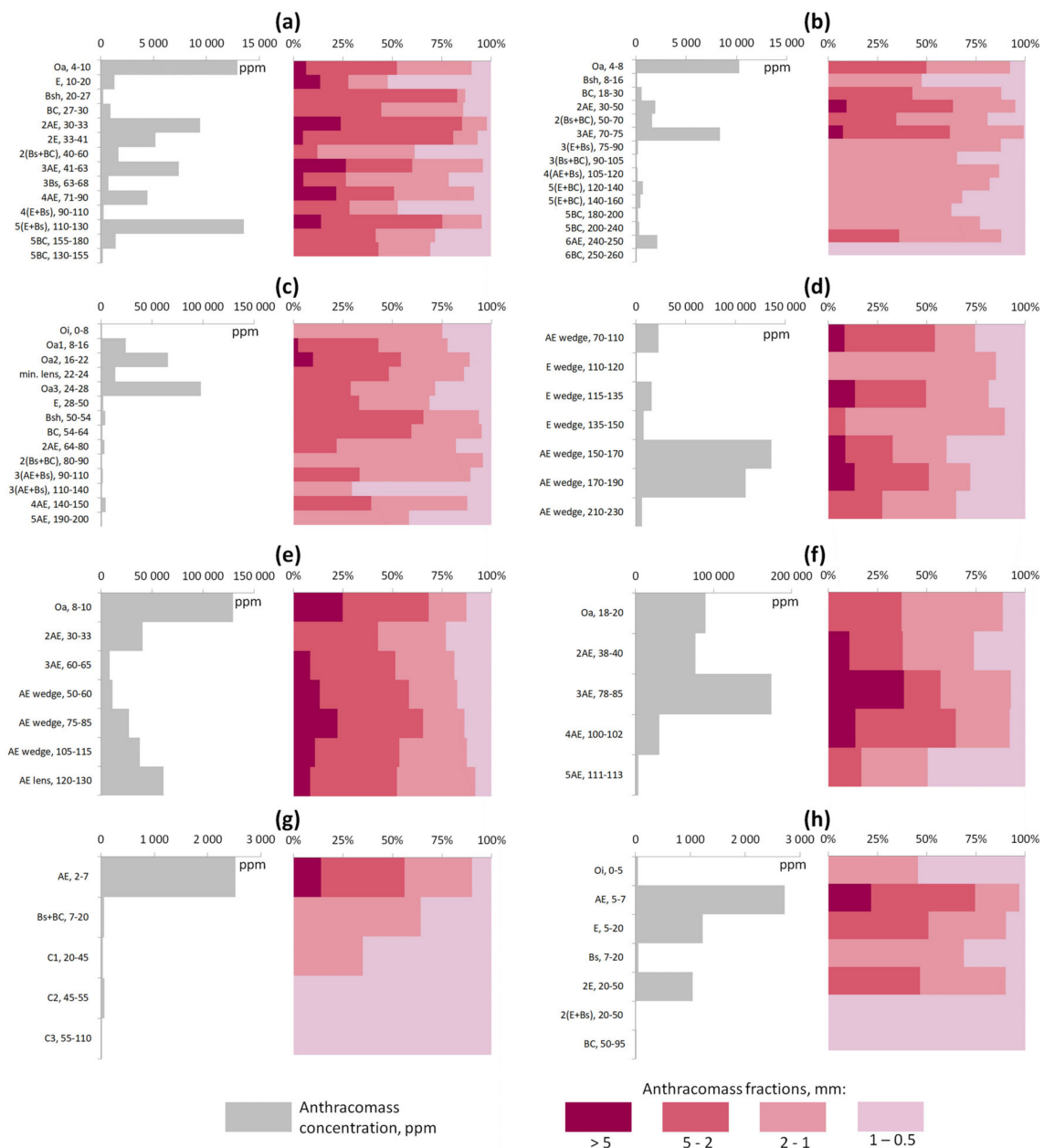
**Figure 3.** Anthracomass distribution in soils of sinkholes and in soils on residual surfaces between sinkholes: (**a**,**b**) periphery of large sinkhole Pin01-18; (**c**) center of sinkhole Pin01-18; (**d**) the charcoal wedge in the channel zone of sinkhole Pin01-18; (**e**,**f**) sinkholes Pin02-18 and Pin03-18; (**g**) Arenosol (Pin04-19) on residual surface between sinkholes with no signs of pedoturbations; (**h**) Podzol (Pin02-19) on residual surface between sinkholes with uprooting features and buried material from horizons E and Bs.
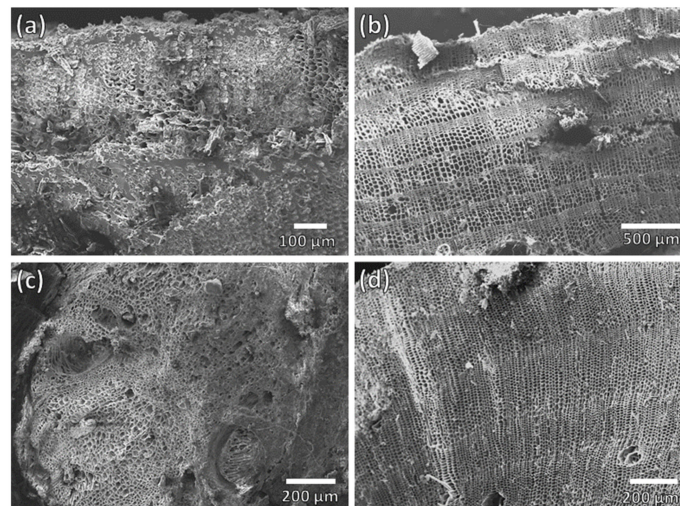
**Figure 4.** Charred plant fragments (scanning electron microscopy in a secondary electron mode): (**a**) tree bark, sinkhole Pin01-18C, depth 9–10 cm; (**b**) pine wood, sinkhole Pin01-18C, depth 30–33 cm; (**c**) tree root, sinkhole Pin01-18C, depth 71–90 cm; (**d**) pine wood, sinkhole Pin02-18, depth 111–112 cm.

## 3.3. Carbon and Nitrogen in Soil and Charcoal

The material of E, Bs, Bsh, and BC soil horizons, including those within buried profiles, contained $0.54 \pm 0.67\%$ TOC and $0.07 \pm 0.03\%$ TN and demonstrated C/N values of $7 \pm 5$. The largest charcoal particles (8–24 mm) selected manually from these subsoil horizons contained $60.68 \pm 9.63\%$ TOC and $0.36 \pm 0.12\%$ TN, while the C/N values reached 390–460. The TOC content determined in the wet-sieved fractions of anthracomass (>5, 5–2, 2–1, 1–0.5 mm) gradually decreased with a reduced size of charcoal particles $41.51 \pm 11.58\%$ (fraction >5 mm), $36.41 \pm 15.81\%$ (5–2 mm), $29.42 \pm 14.40\%$ (2–1 mm), and $24.08 \pm 15.69\%$ (1–0.5 mm), although the nitrogen content did not differ significantly between the fractions $-0.17 \pm 0.06\%$, $0.17 \pm 0.08\%$, $0.18 \pm 0.10\%$, and $0.14 \pm 0.11\%$, respectively. From the coarse fraction to the fine fraction, the C/N values decreased from 329 to 204. With a greater depth, we also observed a weak declining trend in TOC and TN content in each fraction individually (Figure 5), while the C/N ratio within each fraction varied to a lesser extent. In general, the deep subsoil horizons (>150 cm) still contained large amount of anthracomass, suggesting potential pedogenic sources of the paleofire information. Moreover, in some large charcoal pieces (>8 mm) obtained from deep subsoil horizons, the organic carbon content reached 64.87% (nitrogen 0.34%) and remained within the range of 24.75–46.36% (nitrogen 0.15–0.36%) in smaller charcoal fractions (<5 mm).
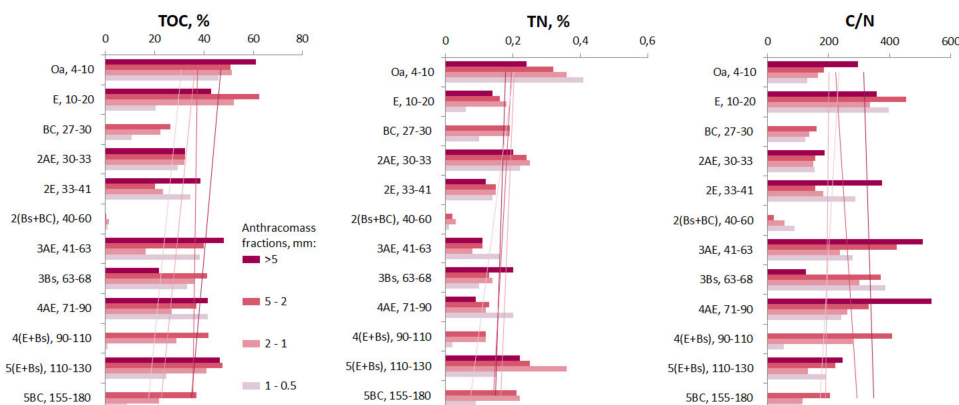


**Figure 5.** Organic carbon, nitrogen and C/N distribution along anthracomass fractions (>5, 5–2, 2–1, 1–0.5 mm fractions) in soil profile of sinkhole Pin01-18 (C section). Lines indicate trends for each fraction.

### 3.4. Carbon and Nitrogen Stable Isotope Ratio

The estimates of carbon and nitrogen stable isotope ratios were obtained both in the anthracomass (pieces > 0.5 mm) and soil material (<2 mm) without anthracomass, all from the same layers. In contrast to C and N concentrations, the ratios of their stable isotopes varied to a lesser extent: $\delta^{13}C = -26.3 \pm 1.0‰$ and $\delta^{15}N = -0.6 \pm 0.9‰$ for anthracomass; $\delta^{13}C = -25.9 \pm 0.6‰$ and $\delta^{15}N = -3.3 \pm 2.4‰$ for soil material. The $\delta^{13}C$ ranges plotted at means ± 1 standard deviation overlapped for soils and macrocharcoal, although the range for soil material was narrower (Figure 6). For the most part, the charcoal and soil material differed in $\delta^{15}N$ values, which are sensitive to the high-temperature influence.
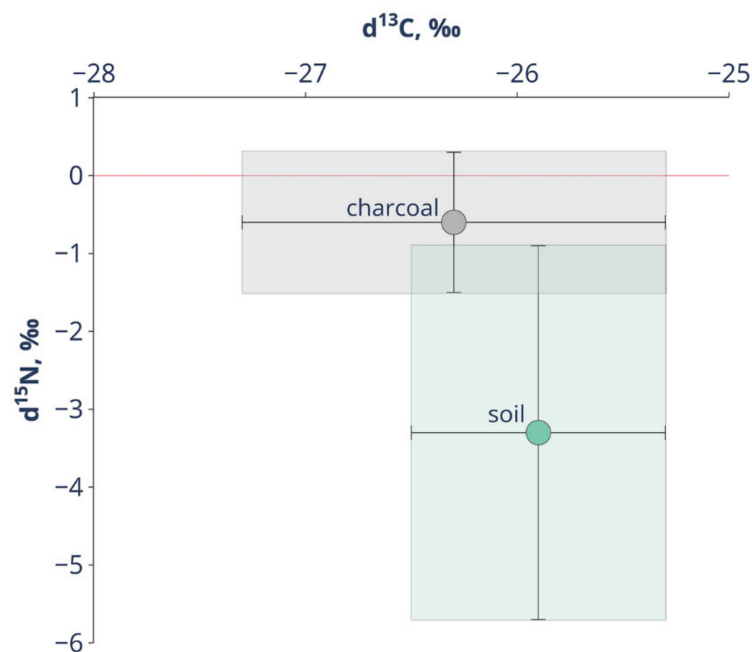


**Figure 6.** Carbon and nitrogen stable isotope ratios in anthracomass and soil material (plotted at mean ± 1 standard deviation).

### 3.5. Radiocarbon Data

The maximum temporal "depth" of pyrogenic soil archives in sinkholes was estimated from the radiocarbon dating of macrocharcoal particles and reached 10,260 ± 35 cal BP (Figures 7 and 8, Table S2). The youngest dates were obtained for charcoals from Oa horizons with $^{14}C$ ages of 120 ± 75 and 80 ± 65 cal BP, indicating that they had captured the fire events of the ~20th century also present within our dendrochronological dataset (see Section 3.6). The summed probability distributions of the 37 radiocarbon dates (Figure 8a) demonstrate lengthy periods with a higher frequency of recurring fires at 10,000–9000 cal BP, 7500–6400 cal BP, 4000–2800 cal BP, 2300–0 cal BP and with a putative fire-depleted interval at ~5500–4000 cal BP. The average interval between means of calibrated radiocarbon ranges for the whole dataset was 283 ± 269 years. In the last 1000 years the interval has decreased to 117 ± 114 years, whereas in the previous 9200 years it was 330 ± 283 years.

The shape and size of sinkholes strongly affected the deposition modes and rates (Figure 7), suggesting that the soil charcoal archives in sinkholes of various dimensions should be used as complementary proxies. The oldest date received (sinkhole Pin01-18, 10,260 ± 35 cal BP) was obtained from the macrocharcoal at the depth of only 140–160 cm, while the deeper layers (160–250 cm) of the same sinkhole contained younger charcoals of 9525 ± 15–9175 ± 60 cal BP. This inversion could not be explained by the "inbuilt age" effect alone, and turbations (e.g., translocation of mineral masses with

the older charcoal from the periphery to the central channel of a sinkhole) are more likely reasons for such a large time discrepancy.

The specific anthracomass concentration (>0.5 mm) was dependent on its age (Figure 8b), with older samples demonstrating lower charcoal abundances. However, 43% of our samples recorded fires in the range of 10,300–5500 cal BP, and we could be confident that our interpretation of temporal trends in fire activity is not limited by a sharp decline in the number of samples through time.
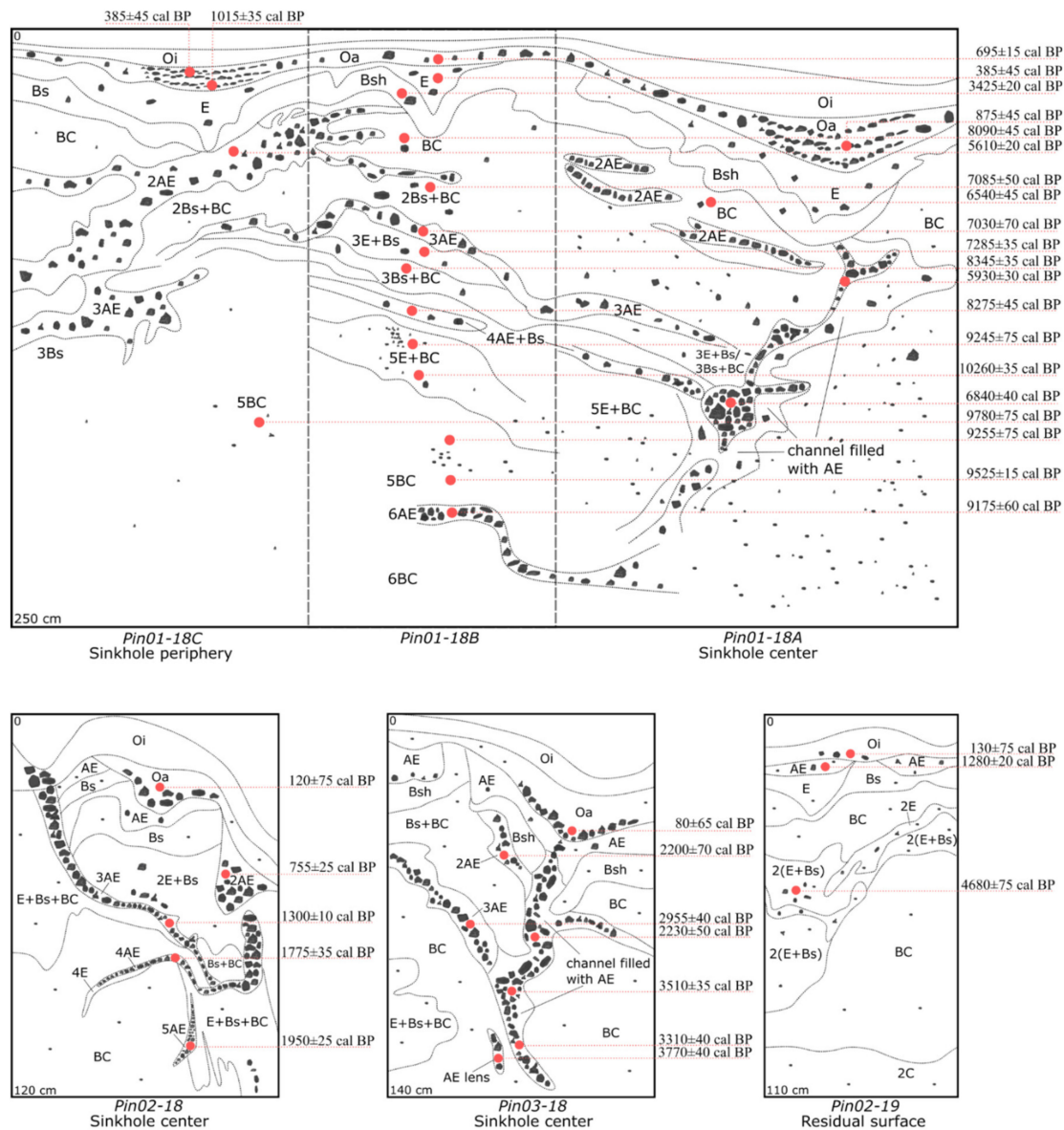


**Figure 7.** Distribution of radiocarbon age (plotted at mean ± 1 sigma, cal BP) for macrocharcoal particles archived in soils of sinkholes (Pin01-18, Pin02-18, Pin03-18) and in soil of residual surface between sinkholes (Pin02-19). For the conventional radiocarbon ages, please refer to Table S2.
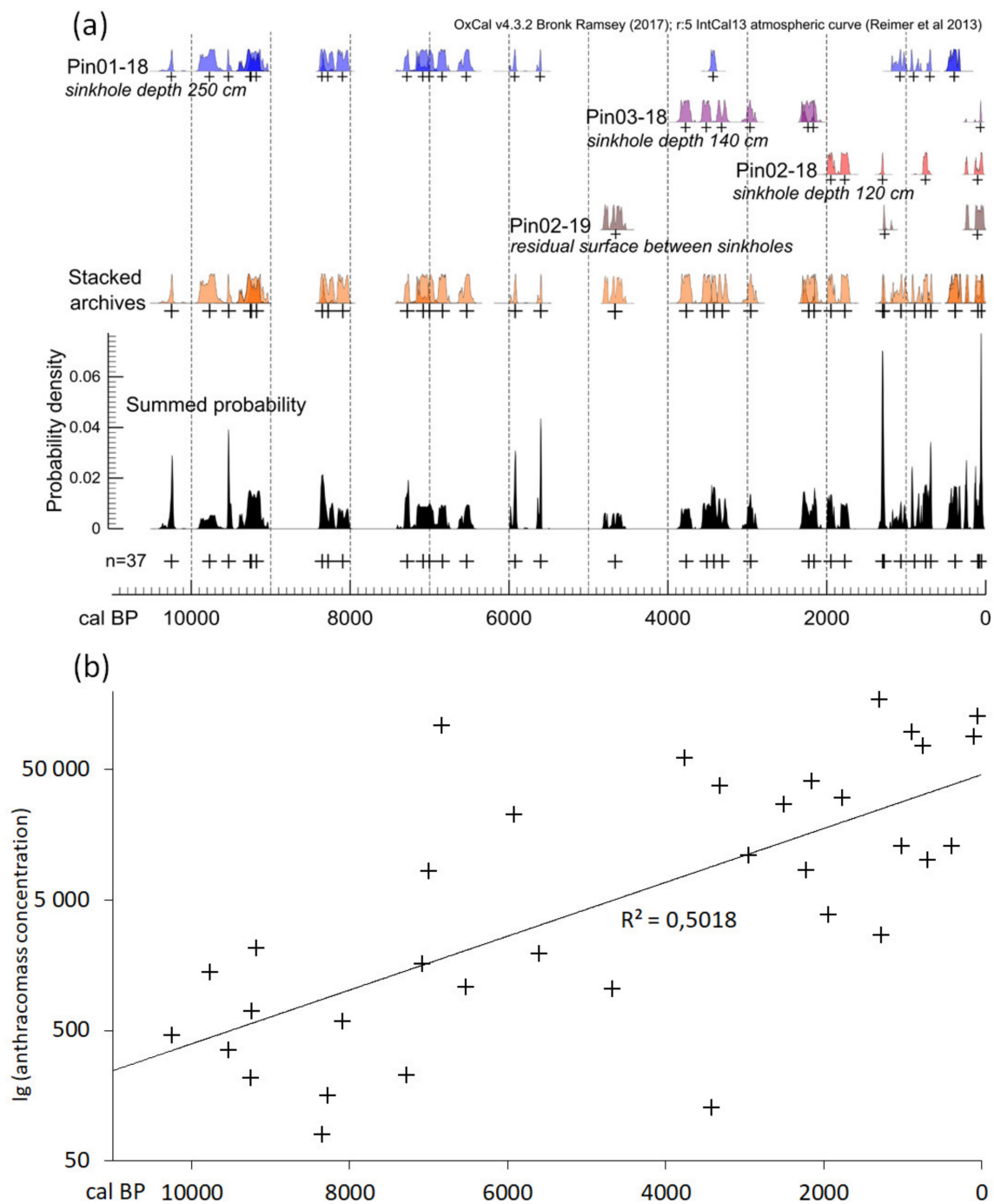
**Figure 8.** Complementary pyrogenic archives in sinkholes of various sizes: (**a**) probability distributions and medians (+) in a set of 37 radiocarbon determinations (macrocharcoal) and (**b**) charcoal concentration (specific anthracomass > 0.5 mm) vs. radiocarbon age of macrocharcoal.

### 3.6. Fire History in the 20th Century (Dendrochronological Detalization)

From the 74 sampled trees, 55 trees exhibited traces of scars in their cores and disks, including two cross-sections with two scars each. The distribution of scars and first sampled ring dates in time is shown in Figure 9. If adjusted for the sampling height and the number of rings to the center of the tree, the dates of the first sampled rings serve as an indicator of the beginning of tree growth, and therefore indicate successions when these dates represent a group. This adjustment equals 10–15 years on average, but even after adjustment these dates are rather approximate. The number of the first sampled

rings increased steadily toward the beginning of the 20th century (Figure 9a,b) and suggests that the main succession for the studied area of the forest occurred at the end of the 19th century.
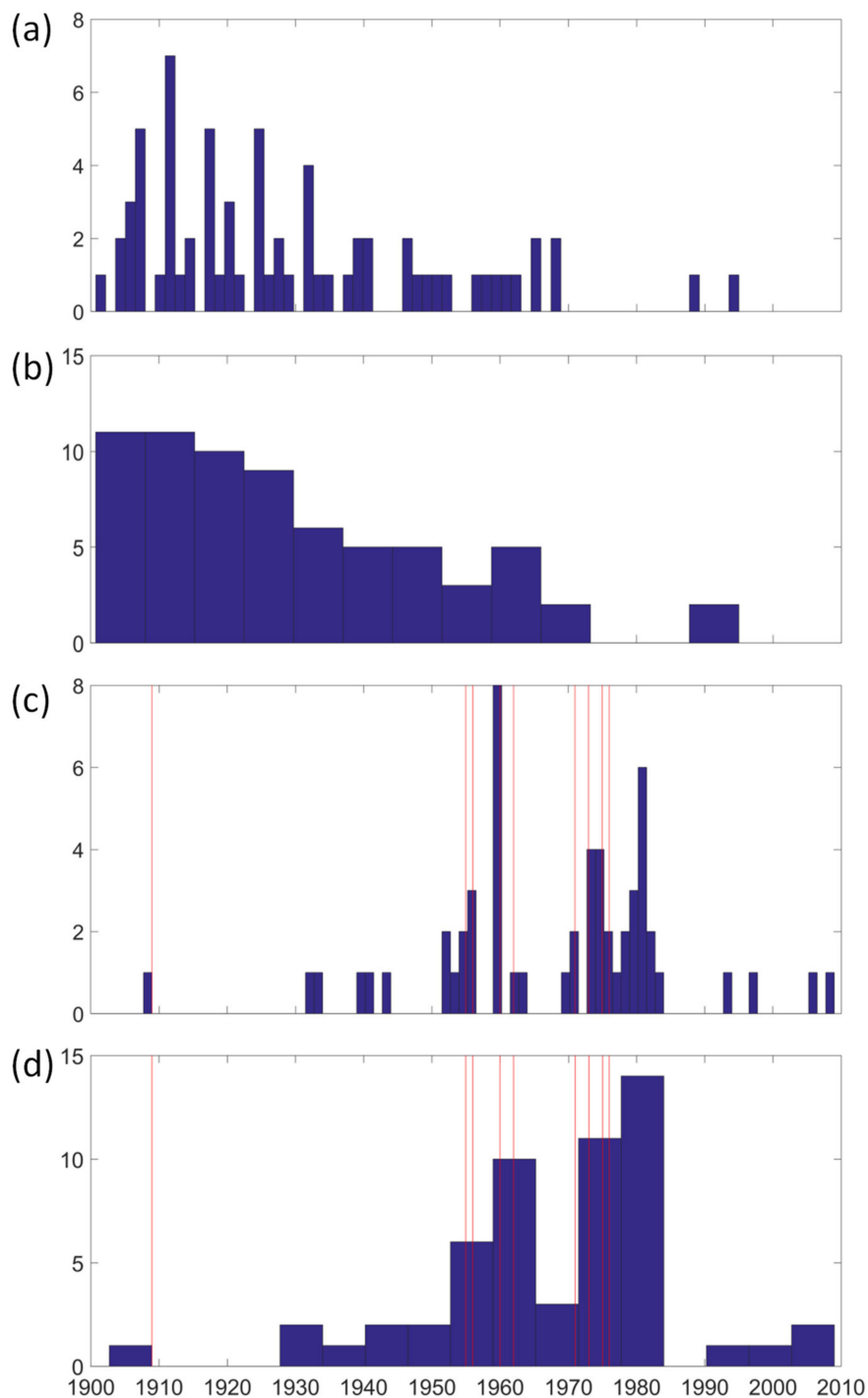


**Figure 9.** Dates of the first sampled tree rings, grouped by 1 year (**a**) and 5 years (**b**); dates of the fire scars grouped by 1 year (**c**) and 5 years (**d**). The number of trees is plotted along the vertical axis, and the red lines indicate the data obtained from the cross-sections, while the rest are from the cores.

Although fire scars were found for every decade since 1900, except for the 1910s–1930s (Figure 9c,d) the maximum number of pyrogenic events (more than five trees with identified fire scars) occurred in 1960, 1974–1975 and 1980–1982, with the last group having 14 trees with scars. Almost all the scars

identified in the cross-sections coincided with one or more scars identified in the cores. The fire of 1960 CE identified in one cross-section, was also identified in core samples of seven trees. This indicates a good accuracy of fire dating using core samples.

## 4. Discussion

### 4.1. Charcoal Burial in Sinkholes

The morphology and stratigraphy (Figure 7) of horizons in the studied pyrogenic archives suggest three major drivers of charcoal burial: (a) paleo and active subsidence/drainage, (b) post-fire erosion/deposition, and (c) uprooting. The soil sequences in sinkholes demonstrate that erosion/deposition is a leading factor in assembling deep pyrogenic archives along topography patterns created by subsidence. This is enhanced by uprooting both during the post-fire disturbance episodes and during continuous tree falls at the stable phases between the fires. These driving forces of charcoal sinking discriminate between karst topography patterns and control the completeness of the macrocharcoal record in soils (Figure 10). The central part of sinkholes surrounding the draining channel comprise the charcoal accumulation *zone 1*, constrained by subsidence and deposition cycles; the slopes at the periphery of sinkholes represent charcoal transportation and accumulation *zone 2*, formed by subsidence, erosion-deposition, and uprooting; while high flats (residual surfaces) between sinkholes constitute charcoal depletion *zone 3*, controlled by erosion and uprooting. These zones alternate within 5–25 m distances and regularly replicate throughout this type of karst landscape.
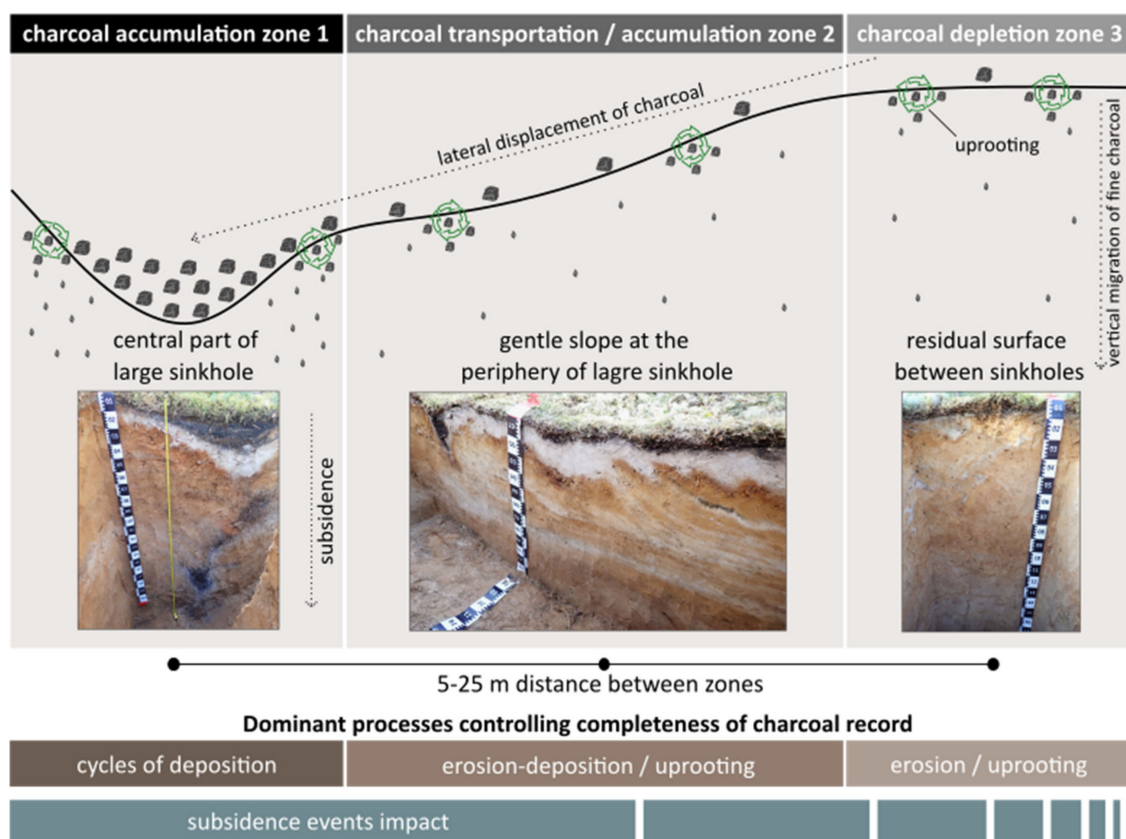


**Figure 10.** Karst topography patterns discriminate between mechanisms of charcoal burial and control completeness of the local macrocharcoal record.

The patterns of anthracomass distribution along the soil profiles confirm our field observations on mechanisms of charcoal burial. However, the laboratory anthracomass calculations additionally suggest that post-fire erosion/deposition and uprooting as major mechanisms of charcoal transportation

to the subsoil are aided by the frontal vertical migration of smaller charcoal particles (<1 mm). The latter were still present in the fluvial and glacial sediments, which underlie the studied soil sequences and were formed before the steady forest ecosystems were established.

### 4.2. Evaluation of the Sinkhole Archives as Paleofire Proxies

Subsidence sinkholes contain well-preserved although very complex (Figure 7) soil records of the local pyrogenic events throughout most of the Holocene. The complexity of these pyrogenic archives is mainly due to an intricate interplay of subsidence, erosion-deposition, and uprooting events with a minor contribution from vertical migration of fine charcoal fractions in the sandy subsoil. We suggest that the soils of the studied karst landscape are less amenable to the extraction of a continuous high-resolution paleofire record of a regional scale in comparison to such sedimentary archives as lake and peat deposits. However, the sinkhole archives surpass other sedimentary records in the amount of in situ pyrogenic "memory", i.e., the data on major fire events and landscape transformations right in the place where the forest was growing and the fire occurred.

Our data indicate a significant long-term PyC sink in soils of the Pinega karst landscape. We found that a vertical distribution of C and N concentrations across the soil archives (individually for each charcoal fraction) is rather stable. Considering that the studied stratum covers ~10,000 years, this proves the high persistence of the anthracomass component in the soil PyC pool. Larger charcoal fractions (>5 and 5–2 mm), as well as individual massive charcoal pieces (8–24 mm) were more stable, as expected, but relatively small fractions (<1 mm) also maintained high TOC and TN concentrations. The C/N ratio did not display a pronounced tendency for decrease with depth within each fraction individually and turned out to be the most stable parameter in the anthracomass of a certain particle size.

$\delta^{13}$C values confirmed the findings obtained from the botanical identification of charcoal pieces and support the hypothesis of a relatively monotonous temporal pattern of vegetation in a consistently drained karst landscape with no abrupt changes during almost the entire Holocene. Stable isotopic composition of the charcoal and soil material differed to the greatest extent in $\delta^{15}$N values. Higher $\delta^{15}$N values in anthracomass can be explained by the fractionation during high temperature impacts [52], while the soil material got subsequently saturated with non-pyrogenic products of plant decay with a $\delta^{15}$N range characteristic of the boreal forest with *Pinus sylvestris*, *Picea abies*, *Vaccinium myrtillus*, *Vaccinium vitis-idaea*, etc. [53].

The maximum temporal "depth" of archives was 10,260 ± 35 cal BP. For the macrocharcoal, 10 out of 37 radiocarbon determinations in a consecutive row demonstrated distances of more than 200 cal BP between 2σ ranges (95.4% probability) of the neighboring determinations (Figure 11). These radiocarbon dates reliably distinguish individual paleofires at a threshold of charcoal "inbuilt age" common to the tree species in the Holocene history of the region. If we only consider soil charcoal radiocarbon dates as a proxy for fire events when they are separated by at least 200-year intervals, this approach provides a minimum estimate of the number of fire events recorded in the sinkhole soil archives throughout most of the Holocene. However, the "inbuilt" age errors are likely significantly smaller at dry sites with fire-prone ecosystems [54], as the karst landscape of this study. Here, the combination of good drainage and fire-prone pine trees may have ensured the increased fire return intervals throughout the Holocene, especially considering long-established factors of lightning occurrence at the Belomor-Kuloy Plateau region [44].

The relative shortage of macrocharcoal material with the radiocarbon ages of ~5500–4000 cal BP (Figures 8a and 11) is likely explained by the low number of sinkholes sampled so far. However, the decline in charcoal accumulation has also been registered around this time in other sedimentary archives, e.g., lake and peat deposits in Scandinavia [55,56] and in Russia [22]. The absence of charcoal particles in soil layers could be explained by climatic parameters, as well as a combination of small amounts of fuel that produced no charcoal (i.e., lichens, mosses, and grasses) and low fire intensity, since the relationship between fuel accumulation and fuel consumption is a key factor that controls the production of charred particles [20,24].
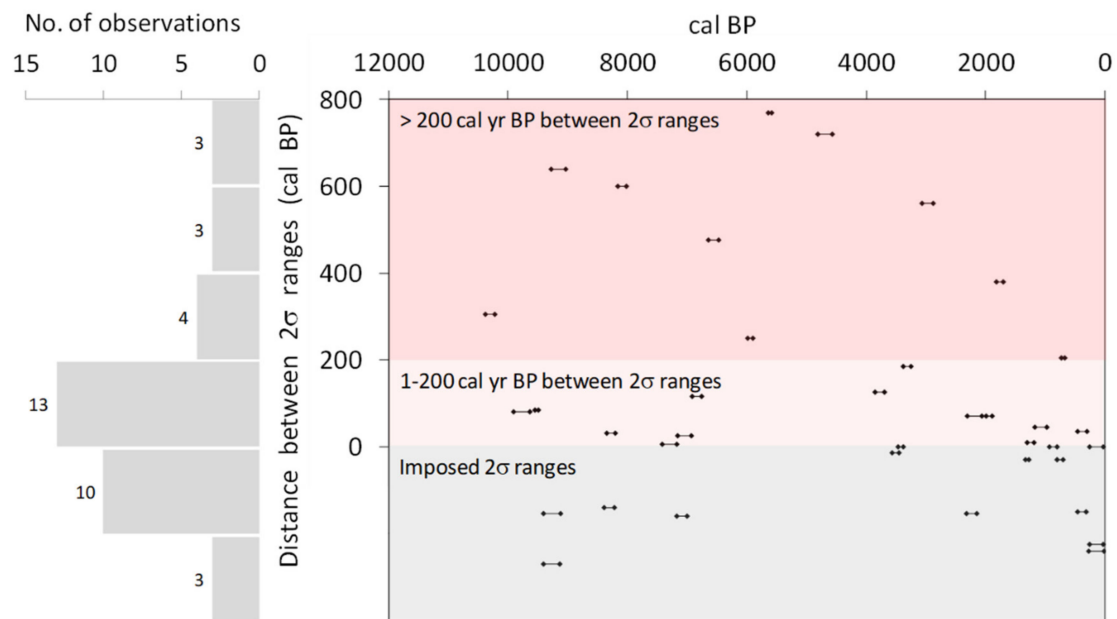
**Figure 11.** Distances between 2σ ranges (cal BP, 95.4% probability) for each $^{14}$C determination in a row of consecutive pyrogenic events (macrocharcoal data).

We compared the radiocarbon ages of organic carbon from soil material (<2 mm) with that of the anthracomass (>0.5 mm) from the same soil layer (Figure 12, Table S2). Although calibrated radiocarbon ranges (cal BP, 2σ, 95.4% probability) could coincide, in most cases $^{14}$C age for TOC from soil was significantly younger than for charcoal from the same layer. There are several possible explanations for this phenomenon. Firstly, the vertical migration of a younger organic matter along the profiles of buried soils in sinkholes, which reduces the estimate of age for soil material. For instance, the greatest discrepancy between the age of charcoal and soil from the same layer was found at a shallow Bsh horizon, which is formed by mutual precipitation of illuviated iron-and carbon-bearing compounds of a modern age. Secondly, the soil-charcoal discrepancy could be connected with the "inbuilt" radiocarbon age in charcoal, which, on the contrary, leads to the overestimation of age. Finally, older charcoal could be introduced into a younger layer by turbations, as well as eroded from soils on residual surfaces, where it was buried by uprooting long ago. These factors could act simultaneously and should be considered carefully when interpreting the data.
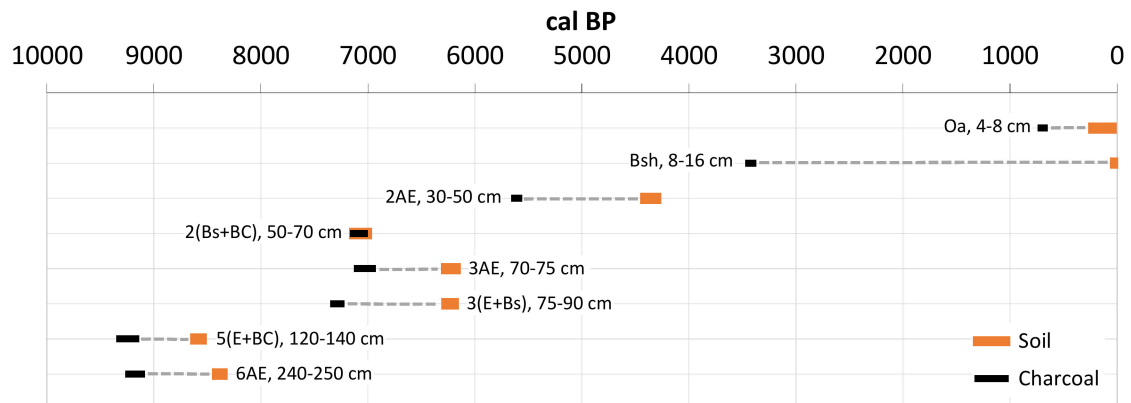


**Figure 12.** Comparison of calibrated radiocarbon ages obtained for macrocharcoal and TOC of soil (<2 mm). The data are plotted for Pin01-18 (B section, see also Table S2) at 2σ ranges (cal BP, 95.4% probability) for each $^{14}$C determination.

### 4.3. Local Paleofire Pattern in a Broader Context

As follows from our data, the fire has been a feature in this karst landscape for millennia, while the record of fossil vegetation is in accordance with the modern plant cover. Soil formation also maintained a rather uniform direction for millennia, and profiles of Podzols regularly replicated. The anthracomass analyses and $\delta^{13}$C values indicate no abrupt changes in vegetation during 10,000 years, and the northern boreal forest dominated by *Pinus* sp. was present in the study area soon after deglaciation. Our data on the important role of pine in the composition of the stand, starting from the Early Holocene, coincide with the results obtained for pollen and wood fragments for this region in other studies [57–60]. However, the proxies that we had in hand do not reliably register short-term post-pyrogenic succession patterns or successions with lower biomass, and hence fuel. When vegetation was represented by a mature forest, which offered a significant amount of fuel, it was stored locally in the sinkhole archives, and we were able to recognize it as macrocharcoal. The high content of macrocharcoal particles and their distribution patterns in the soils of sinkholes indicate that the study area was affected by fires in mature forests throughout most of the Holocene. Regular forest fires in this karst landscape, that is continuously drained by the active sinkhole channels, probably contributed to the maintenance of fire-prone pine forests by cyclic impact. We observed a weak trend in shortening intervals between fires in the last thousand years and obtained detailed information from the dendrochronological dataset for a decadal fire dynamics during the 20th and early 21st centuries. This trend could have arisen at a time when people from Ancient Russia (Novgorod) settled in the region [40] and replaced scarcely distributed old Finnish tribes with an archaic economy [43]. Further detalization of soil records by dendrochronological archives may serve to improve the estimates of fire activity throughout the Holocene. These estimates could be made by the number of injured trees per area and their comparison with charcoal concentrations in the soil for the intersecting periods.

For the boreal forests in the nearby region of Fennoscandia, it was shown previously that the climate explains the highest proportion of variation in vegetation composition, e.g., in Sweden (10,000–4000 cal BP) and in Finland (10,000–1000 cal BP) [61]. A period of climatic warming in the Holocene did not necessarily result in an increased frequency of forest fires [62]. This could be attributed to an increase in summer precipitation, linked to elevated sea surface temperatures and wet westerlies over Fennoscandia [55], while under cool conditions in Scandinavia the frequency of fire-prone periods possibly increased due to the low atmospheric humidity and increased frequency of high-pressure systems dominated by cold and dry air masses [56].

Our data indicate a comparable variation in the fire return intervals during the Holocene to the one established in the relatively close regions of Finland and Northwest Russia [60]: 117–330 years (this study) and 126–237 [60]. Moreover, the putative fire-depleted interval at ~5500–4000 cal BP found in this study corresponds to the relatively low fire activity in the period of 6500–4000 cal BP, with a particular decrease in 5000–4000 cal BP registered in the Kämmekä hollow (Finland) [60].

Popov and Puchnina [33] have previously highlighted that the frequency of forest fires accelerated to one per decade in the late 20th and early 21st centuries at the territory of the Pinega State Nature Reserve adjacent to our study site. Considering the forest protection system in the nature reserve, with controls over the activities of locals, the recent fire frequency shift is explained mainly by the drier climate, with most pyrogenic events originating from dry thunderstorms [33]. Our findings do not contradict climatic interpretations of the long-term fire pattern in the region. However, in the non-protected areas, the decadal dynamics of recent fires derived from the tree-ring data indicates a conspicuous impact of human activities.

## 5. Conclusions

1. A significant long-term PyC sink is present in soils of the karst landscapes at the north of the Archangelsk Region, in Russia. Subsidence sinkholes contain well-preserved although very complicated soil records of the local pyrogenic events throughout most of the Holocene, as well as the data on the stages of soil formation during this period.

2.　The pyrogenic archives in sinkholes were formed and affected by an intricate interplay of subsidence, erosion-deposition, and uprooting events, and their maximum temporal "depth", estimated from the radiocarbon dating of macrocharcoal that reached 10,260 ± 35 cal BP. 10 out of 37 radiocarbon determinations in a consecutive row exhibited distances of more than 200 cal BP between 2σ ranges (95.4% probability) of neighboring determinations. This is beyond a threshold of charcoal "inbuilt age" common to the tree species in the Holocene history of the region, thus reliably distinguishing between individual paleofires.

3.　The intervals between fires have shortened in the last 1000 years (macrocharcoal data), and during the 20th and early 21st centuries fires have occurred almost every decade (tree-ring data). However, the macrocharcoal paleofire proxies could be partially affected by the better quality of the recent material preserved in the soil, turbations, and the "inbuilt" effect of radiocarbon age should thus be complemented by other pyrogenic archives (e.g., in lake/peat sediments) for accurate interpretations.

4.　Soil formation with Podzols established at the inter-pyrogenic stages was reproduced within the ten-thousand-year period. The charcoal record of the three sampled sinkholes suggests that *Pinus* sp. was the dominant tree species across this period.

**Conflicts of Interest:** The authors declare no conflict of interest.

## References

1.　Carcaillet, C.; Thinon, M. Pedoanthracological contribution to the study of the evolution of the upper treeline in the Maurienne Valley (North French Alps): Methodology and preliminary data. *Rev. Palaeobot. Palynol.* **1996**, *91*, 399–416. [CrossRef]

2.　Gavin, D.G. Estimation of inbuilt age in radiocarbon ages of soil charcoal for fire history studies. *Radiocarbon* **2001**, *43*, 27–44. [CrossRef]

3.　Gavin, D.G.; Brubaker, L.B.; Lertzman, K.P. Holocene fire history of a coastal temperate rain forest based on soil charcoal radiocarbon dates. *Ecology* **2003**, *84*, 186–201. [CrossRef]

4.　Lertzman, K.; Gavin, D.; Hallett, D.; Brubaker, L.; Lepofsky, D.; Mathewes, R. Long-term fire regime estimated from soil charcoal in coastal temperate rainforests. *Conserv. Ecol.* **2002**, *6*, 1–13. Available online: https://www.jstor.org/stable/26271885 (accessed on 27 November 2020). [CrossRef]

5.　Talon, B. Reconstruction of Holocene high-altitude vegetation cover in the French southern Alps: Evidence from soil charcoal. *Holocene* **2010**, *20*, 35–44. [CrossRef]

6.　Talon, B.; Payette, S.; Filion, L.; Delwaide, A. Reconstruction of the long-term fire history of an old-growth deciduous forest in Southern Québec, Canada, from charred wood in mineral soils. *Quat. Res.* **2005**, *64*, 36–43. [CrossRef]

7.　Touflan, P.; Talon, B.; Walsh, K. Soil charcoal analysis: A reliable tool for spatially precise studies of past forest dynamics: A case study in the French southern Alps. *Holocene* **2010**, *20*, 45–52. [CrossRef]

8.　Novák, J.; Sádlo, J.; Svobodová-Svitavská, H. Unusual vegetation stability in a lowland pine forest area (Doksy region, Czech Republic). *Holocene* **2012**, *22*, 947–955. [CrossRef]

9.　Robin, V.; Nelle, O. Contribution to the reconstruction of central European fire history, based on the soil charcoal analysis of study sites in northern and central Germany. *Veg. Hist. Archaeobot.* **2014**, *23*, 51–65. [CrossRef]

10.　Robin, V.; Rickert, B.H.; Nadeau, M.J.; Nelle, O. Assessing Holocene vegetation and fire history by a multiproxy approach: The case of Stodthagen Forest (Northern Germany). *Holocene* **2012**, *22*, 337–346. [CrossRef]

11.　Compostella, C.; Trombino, L.; Caccianiga, M. Late Holocene soil evolution and treeline fluctuations in the Northern Apennines. *Quat. Int.* **2013**, *289*, 46–59. [CrossRef]

12.　Dyakonov, K.N.; Novenko, E.Y.; Mironenko, I.V.; Kuprijanov, D.A.; Bobrovsky, M.V. The role of fires in the Holocene landscape dynamics of the southeastern part of Meshchera Lowlands. *Dokl. Earth Sci.* **2017**, *477*, 1336–1342. [CrossRef]

13.　Bobrovsky, M.V.; Kupriaynov, D.A.; Khanina, L.G. Anthracological and morphological analysis of soils for the reconstruction of the forest ecosystem history (Meshchera Lowlands, Russia). *Quat. Int.* **2019**, *516*, 70–82. [CrossRef]

14.　Bird, M.I.; Wynn, J.G.; Saiz, G.; Wurster, C.M.; McBeath, A. The pyrogenic carbon cycle. *Annu. Rev. Earth Planet. Sci.* **2015**, *43*, 273–298. [CrossRef]

15.　Reisser, M.; Purves, R.S.; Schmidt, M.W.; Abiven, S. Pyrogenic carbon in soils: A literature-based inventory and a global estimation of its content in soil organic carbon and stocks. *Front. Earth Sci.* **2016**, *4*, 80. [CrossRef]

16.　Jones, M.W.; Santín, C.; van der Werf, G.R.; Doerr, S.H. Global fire emissions buffered by the production of pyrogenic carbon. *Nat. Geosci.* **2019**, *12*, 742–747. [CrossRef]

17.　Shakesby, R.A.; Doerr, S.H. Wildfire as a hydrological and geomorphological agent. *Earth-Sci. Rev.* **2006**, *74*, 269–307. [CrossRef]

18.　Abney, R.B.; Berhe, A.A. Pyrogenic carbon erosion: Implications for stock and persistence of pyrogenic carbon in soil. *Front. Earth Sci.* **2018**, *6*, 26. [CrossRef]

19.　Clark, J.S. Particle motion and the theory of charcoal analysis: Source area, transport, deposition, and sampling. *Quat. Res.* **1988**, *30*, 67–80. [CrossRef]

20.　Clark, J.S.; Lynch, J.; Stocks, B.J.; Goldammer, J.G. Relationships between charcoal particles in air and sediments in west-central Siberia. *Holocene* **1998**, *8*, 19–29. [CrossRef]

21.　Barhoumi, C.; Peyron, O.; Joannin, S.; Subetto, D.; Kryshen, A.; Drobyshev, I.; Girardin, M.P.; Brossier, B.; Paradis, L.; Pastor, T.; et al. Gradually increasing forest fire activity during the Holocene in the northern Ural region (Komi Republic, Russia). *Holocene* **2019**, *29*, 1906–1920. [CrossRef]

22.　Kupriyanov, D.A.; Novenko, E.Y. Reconstruction of the Holocene Dynamics of Forest Fires in the Central Part of Meshcherskaya Lowlands According to Antracological Analysis. *Contemp. Probl. Ecol.* **2019**, *12*, 204–212. [CrossRef]

23.　Magne, G.; Brossier, B.; Gandouin, E.; Paradis, L.; Drobyshev, I.; Kryshen, A.; Hély, C.; Alleaume, S.; Ali, A.A. Lacustrine charcoal peaks provide an accurate record of surface wildfires in a North European boreal forest. *Holocene* **2019**, *30*, 380–388. [CrossRef]

24.　Ohlson, M.; Tryterud, E. Interpretation of the charcoal record in forest soils: Forest fires and their production and deposition of macroscopic charcoal. *Holocene* **2000**, *10*, 519–525. [CrossRef]

25.　Tinner, W.; Hofstetter, S.; Zeugin, F.; Conedera, M.; Wohlgemuth, T.; Zimmermann, L.; Zweifel, R. Long-distance transport of macroscopic charcoal by an intensive crown fire in the Swiss Alps-implications for fire history reconstruction. *Holocene* **2006**, *16*, 287–292. [CrossRef]

26.　Marlon, J.R.; Bartlein, P.J.; Daniau, A.L.; Harrison, S.P.; Maezumi, S.Y.; Power, M.J.; Tinner, W.; Vanniére, B. Global biomass burning: A synthesis and review of Holocene paleofire records and their controls. *Quat. Sci. Rev.* **2013**, *65*, 5–25. [CrossRef]

27.　Marlon, J.R.; Kelly, R.; Daniau, A.L.; Vannière, B.; Power, M.J.; Bartlein, P.; Higuera, P.; Blarquez, O.; Brewer, S.; Brücher, T.; et al. Reconstructions of biomass burning from sediment charcoal records to improve data-model comparisons. *Biogeosciences* **2016**, *13*, 3225–3244. [CrossRef]

28. Novenko, E.Y.; Tsyganov, A.N.; Volkova, E.M.; Kupriyanov, D.A.; Mironenko, I.V.; Babeshko, K.V.; Utkina, A.S.; Popov, V.; Mazei, Y.A. Mid-and Late Holocene vegetation dynamics and fire history in the boreal forest of European Russia: A case study from Meshchera Lowlands. *Palaeogeogr. Palaeoclimatol. Palaeoecol.* **2016**, *459*, 570–584. [CrossRef]

29. Novenko, E.Y.; Tsyganov, A.N.; Mazei, N.G.; Kupriyanov, D.A.; Rudenko, O.V.; Bobrovsky, M.V.; Erman, N.M.; Nizovtsev, V.A. Palaeoecological evidence for climatic and human impacts on vegetation in the temperate deciduous forest zone of European Russia during the last 4200 years: A case study from the Kaluzhskiye Zaseki Nature Reserve. *Quat. Int.* **2019**, *516*, 58–69. [CrossRef]

30. Feurdean, A.; Florescu, G.; Tanţău, I.; Vannière, B.; Diaconu, A.C.; Pfeiffer, M.; Warren, D.; Hutchinson, S.M.; Gorina, N.; Gałka, M.; et al. Recent fire regime in the southern boreal forests of western Siberia is unprecedented in the last five millennia. *Quat. Sci. Rev.* **2020**, *244*, 106495. [CrossRef]

31. Cabadas-Báez, H.; Solleiro-Rebolledo, E.; Sedov, S.; Pi-Puig, T.; Gama-Castro, J. Pedosediments of karstic sinkholes in the eolianites of NE Yucatán: A record of Late Quaternary soil development, geomorphic processes and landscape stability. *Geomorphology* **2010**, *122*, 323–337. [CrossRef]

32. Meyer-Heintze, S.; Sprafke, T.; Krech, M.; Beigel, R.; Nadler, M.; Kriens, B.; Wagner, F.; Solleiro-Rebolledo, E.; Damm, B.; Falkenstein, F.; et al. Pedosedimentary and geoarcheological archives from clay-dominated sinkhole infillings in Middle Franconia, Germany. *Catena* **2020**, *195*, 104893. [CrossRef]

33. Popov, S.Y.; Puchnina, L.V. Disturbance map of Pinega State Reserve vegetation cover in XVIII-XXI cent. *Sovrem. Probl. Distantsionnogo Zondirovaniya Zemli Kosm.* **2017**, *14*, 147–156. (In Russian) [CrossRef]

34. Goryachkin, S.V.; Pfeiffer, E.-M. (Eds.) Soils and perennial underground ice of glaciated and karst landscapes in northern European Russia. In *Guidebook for the Field Session of the IV International Conference on Cryopedology*; Institute of Geography RAS: Moscow, Russia, 2005.

35. Shavrina, E.V.; Malkov, V.N.; Gurkalo, E.I. Karst development and distribution in the Arkhangelsk Region. *Geomorfologiya* **2007**, *2*, 90–101. (In Russian) [CrossRef]

36. Demidov, I.N.; Houmark-Nielsen, M.; Kjaer, K.H.; Larsen, E. The last Scandinavian Ice Sheet in northwestern Russia: Ice flow patterns and decay dynamics. *Boreas-Int. J. Quat. Res.* **2006**, *35*, 425–443. [CrossRef]

37. Yelovicheva, Y.K. Conditions of Holocene carbonates deposition in Arkhangelsk region. In *Lake Carbonates of Non-Chernosemic Zone of USSR*; PPI: Perm, Russia, 1985; pp. 69–78. (In Russian)

38. Zubovich, S.F.; Kokarovtsev, V.K.; Uspenskaya, O.N. Holocene climate of north of Non-chernosemic zone of European part of USSR (on example of Arkhangelsk region). In *Paleoclimates of Holocene on European Part of USSR*; Nauka: Moscow, USSR, 1988. (In Russian)

39. Popov, S.Y. Structure and features of spatial distribution of pine forests in the Pinega State Nature Reserve. *Nat. Conserv. Res.* **2017**, *2*, 40–56. (In Russian) [CrossRef]

40. Makarov, N.A. *Colonization of the Northern Periphery of Ancient Russia, 1000–1300 A.D*; Scriptorium: Moscow, Russia, 1997; 386p, (In Russian with extended summary in English).

41. Tallavaara, M.; Pesonen, P.; Oinonen, M. Prehistoric population history in eastern Fennoscandia. *J. Archaeol. Sci.* **2010**, *37*, 251–260. [CrossRef]

42. Tallgren, A.M. Die russischen und asiatischen archäologischen. Sammlungen im Nationalmuseum Finnlands. *Eurasia Septentr. Antiq.* **1928**, *3*, 141–164.

43. Tallgren, A.M. Biarmia. *Eurasia Septentr. Antiq.* **1931**, *6*, 100–120.

44. Burlakov, P.S.; Khmara, K.A. Lightning ignited forest fires as a geoecological factor influencing the stability of light coniferous forests of the Soyana river basin on Belomorsko-Kuloyskoe plateau. *Tr. Karel. Nauchnogo Cent. Ras.* **2011**, *1*, 48–53. (In Russian)

45. Stokes, M.A.; Smiley, T.L. *An Introduction to Tree-Ring Dating*; University of Arizona Press: Tucson, AZ, USA, 1968.

46. Barefoot, A.C.; Hankins, F.W. *Identification of Modern and Tertiary Woods*; Oxford University Press: New York, NY, USA, 1982; 189p.

47. Vikhrov, B.E. *Diagnostic Signs of Wood of the Main Forestry and Timber Industry Species of the USSR*; Academy of Sciences Publishing House: Moscow, USSR, 1959; 131p. (In Russian)

48. Ramsey, C.B. Bayesian analysis of radiocarbon dates. *Radiocarbon* **2009**, *51*, 337–360. [CrossRef]

49. Paula, J.R.; Edouard, B.A.; Bayliss, J.; Warren, B.; Paul, G. IntCal13 and Marine13 radiocarbon age calibration curves 0–50,000 years cal BP. *Radiocarbon* **2013**, *55*, 1869–1887. [CrossRef]

50. Hua, Q.; Barbetti, M.; Rakowski, A. Atmospheric radiocarbon for the period 1950–2010. *Radiocarbon* **2013**, *55*, 2059–2072. [CrossRef]

51. IUSS Working Group WRB. *World Reference Base for Soil Resources 2014, Update 2015 International Soil Classification System for Naming Soils and Creating Legends for Soil Maps*; World Soil Resources Reports 106; FAO: Rome, Italy, 2015; Available online: http://www.fao.org/3/a-i3794en.pdf (accessed on 27 November 2020).

52. Turekian, V.C.; Macko, S.; Ballentine, D.; Swap, R.J.; Garstang, M. Causes of bulk carbon and nitrogen isotopic fractionations in the products of vegetation burns: Laboratory studies. *Chem. Geol.* **1998**, *152*, 181–192. [CrossRef]

53. Hyodo, F.; Kusaka, S.; Wardle, D.A.; Nilsson, M.C. Changes in stable nitrogen and carbon isotope ratios of plants and soil across a boreal forest fire chronosequence. *Plant Soil* **2013**, *364*, 315–323. [CrossRef]

54. Hoffman, K.M.; Gavin, D.G.; Lertzman, K.P.; Smith, D.J.; Starzomski, B.M. 13,000 years of fire history derived from soil charcoal in a British Columbia coastal temperate rain forest. *Ecosphere* **2016**, *7*, e01415. [CrossRef]

55. Carcaillet, C.; Bergman, I.; Delorme, S.; Hornberg, G.; Zackrisson, O. Long-term fire frequency not linked to prehistoric occupations in northern Swedish boreal forest. *Ecology* **2007**, *88*, 465–477. [CrossRef]

56. Drobyshev, I.; Bergeron, Y.; De Vernal, A.; Moberg, A.; Ali, A.A.; Niklasson, M. Atlantic SSTs control regime shifts in forest fire activity of Northern Scandinavia. *Sci. Rep.* **2016**, *6*, 22532. [CrossRef]

57. Binney, H.A.; Willis, K.J.; Edwards, M.E.; Bhagwat, S.A.; Anderson, P.M.; Andreev, A.A.; Blaauw, M.; Damblon, F.; Haesaerts, P.; Kienast, F.; et al. The distribution of late-Quaternary woody taxa in northern Eurasia: Evidence from a new macrofossil database. *Quat. Sci. Rev.* **2009**, *28*, 2445–2464. [CrossRef]

58. MacDonald, G.M.; Velichko, A.A.; Kremenetski, C.V.; Andreev, A. Holocene treeline history and climate change across northern Eurasia. *Quat. Res.* **2000**, *53*, 302–311. [CrossRef]

59. Salonen, J.S.; Seppä, H.; Väliranta, M.; Jones, V.J.; Self, A.; Heikkilä, M.; Kultti, S.; Yang, H. The Holocene thermal maximum and late-Holocene cooling in the tundra of NE European Russia. *Quat. Res.* **2011**, *75*, 501–511. [CrossRef]

60. Stivrins, N.; Aakala, T.; Ilvonen, L.; Pasanen, L.; Kuuluvainen, T.; Vasander, H.; Gałka, M.; Disbrey, H.R.; Liepins, J.; Holmström, L.; et al. Integrating fire-scar, charcoal and fungal spore data to study fire events in the boreal forest of northern Europe. *Holocene* **2019**, *29*, 1480–1490. [CrossRef]

61. Kuosmanen, N.; Marquer, L.; Tallavaara, M.; Molinari, C.; Zhang, Y.; Alenius, T.; Edinborough, K.; Pesonen, P.; Reitalu, T.; Renssen, H.; et al. The role of climate, forest fires and human population size in Holocene vegetation dynamics in Fennoscandia. *J. Veg. Sci.* **2018**, *29*, 382–392. [CrossRef]

62. Pitkänen, A.; Huttunen, P.; Jungner, H.; Tolonen, K. A 10,000 year local forest fire history in a dry heath forest site in eastern Finland, reconstructed from charcoal layer records of a small mire. *Can. J. For. Res.* **2002**, *32*, 1875–1880. [CrossRef]